Microfluidic rheology of active particle suspensions: Kinetic theory

Roberto Alonso-Matilla, Barath Ezhilan, and David Saintillan
Department of Mechanical and Aerospace Engineering, University of California San Diego, 9500 Gilman Drive, La Jolla, California 92093, USA

(Received 31 March 2016; accepted 4 June 2016; published online 17 June 2016)

We analyze the effective rheology of a dilute suspension of self-propelled slender particles confined between two infinite parallel plates and subject to a pressure-driven flow. We use a continuum kinetic model to describe the configuration of the particles in the system, in which the disturbance flows induced by the swimmers are taken into account, and use it to calculate estimates of the suspension viscosity for a range of channel widths and flow strengths typical of microfluidic experiments. Our results are in agreement with previous bulk models, and in particular, demonstrate that the effect of activity is strongest at low flow rates, where pushers tend to decrease the suspension viscosity whereas pullers enhance it. In stronger flows, dissipative stresses overcome the effects of activity leading to increased viscosities followed by shear-thinning. The effects of confinement and number density are also analyzed, and our results confirm the apparent transition to superfluidity reported in recent experiments on pusher suspensions at intermediate densities. We also derive an approximate analytical expression for the effective viscosity in the limit of weak flows and wide channels, and demonstrate good agreement between theory and numerical calculations. *Published by AIP Publishing*. [http://dx.doi.org/10.1063/1.4954193]

I. INTRODUCTION

The transport of motile cells and other self-propelled swimmers through small-scale microfluidic devices has received much scrutiny over the last decade, in part due to its relevance to biological processes such as reproduction[1–3] and its use in engineering applications such as cell sorting and cell concentration.[4–7] Unlike passive particles whose transport is largely dictated by the imposed flow, the case of active swimmers is significantly more complex due to their self-propulsion, which enables them to swim across streamlines and can cause them to accumulate at boundaries.[8–10] In the presence of shear, the coupling of self-propulsion and alignment of slender swimmers with the flow has also been shown to result in unexpected transport phenomena such as upstream swimming[3,11,12] and migration from low-shear towards high-shear regions in pressure-driven channel flows.[13] Such effects occur even in very dilute suspensions when interparticle interactions are negligible.

As a result of their swimming kinematics, microorganisms also exert active stresses on the carrying fluid, thereby driving local disturbance flows that have been characterized experimentally.[14–16] Many microorganisms are nearly neutrally buoyant, so that the leading-order disturbance that they drive in the surrounding medium is a dipole flow, which can be interpreted as resulting from the equal and opposite thrust and drag forces exerted by the flagella and cell body on the fluid, respectively. When placed in an external flow, these disturbances can either facilitate or hinder the flow depending on the sign of the dipole strength σ_0 and on its orientation relative to the flow, potentially leading to unusual rheologies. This was first noted in a theoretical study by Hatwalne *et al.*,[17] who argued that extensile particles or so-called pushers for which $\sigma_0 < 0$ should have a negative intrinsic viscosity $[\eta] < 0$, whereas contractile particles or pullers for which $\sigma_0 > 0$ should have $[\eta] > 0$. A number of more sophisticated models have been proposed since,[18–26] which usually extend theories for the rheology of passive rod

suspensions[27–29] to account for this active dipole and have led to similar predictions. Of particular relevance to the present study is the model of Saintillan,[20] which calculated the effective viscosity and normal stress differences in a dilute active suspension in uniform shear flow as functions of shear rate. The model showed that the effects of activity are strongest in weak flows, where a reduction in viscosity occurs in pusher suspensions; in stronger flows, dissipative viscous stresses were shown to overtake active stresses and lead to a positive intrinsic viscosity followed by shear-thinning.

Experiments aimed at testing these predictions have been relatively scarce, in part owing to technical difficulties: first, the effects of activity on the rheology are strongest at very low shear rates, which are not accessible to standard rheometers; second, the viscosity of dilute suspensions is typically close to that of water, whereas rheometers work best with more viscous fluids. Nonetheless, a few experimental techniques have been devised to overcome these challenges. In the case of suspensions of pusher particles, Sokolov and Aranson[30] were the first to estimate the viscosity of thin liquid films containing swimming *Bacillus subtilis* by measuring the angular velocity of a rotating particle subject to a constant imposed magnetic torque. They indeed reported a viscosity reduction due to activity, which initially became stronger with increasing volume fraction. However, the unusual nature of their experimental setup rendered quantitative comparisons with bulk models difficult. Very recently, López *et al.*[31] performed experiments in a circular Couette cell specially designed to measure torques at very low shear rates, and confirmed the existence of a negative intrinsic viscosity in suspensions of *Escherichia coli*. In the low-shear-rate plateau, they found that the total viscosity could even decrease to zero in sufficiently concentrated suspensions, suggesting that active pusher suspensions can behave as superfluids. The possibility of a negative total viscosity is consistent with other experiments[32,33] as well as theories[34–36] that have reported spontaneous unidirectional flows in confined active suspensions; in the case of bulk suspensions, the predicted decrease of the intrinsic zero-shear-rate viscosity towards zero has also been shown to be the driver of hydrodynamic instabilities leading to collective motion.[37]

The case of puller particles was considered by Rafaï *et al.*,[38] who studied suspensions of the micro alga *Chlamydomonas reinhardtii*. They used concentrated suspensions in a cone-plate rheometer and measured higher shear viscosities in suspensions of live cells than in suspensions of dead cells as predicted by models. The extensional rheology of both pusher and puller suspensions was also recently studied by McDonnell *et al.*[39] using an acoustically driven microfluidic capillary-breakup extensional rheometer. In agreement with studies in shear flows and with theoretical predictions in extensional flows,[21] they observed a decrease in viscosity in bacterial and sperm suspensions but an increase in algae suspensions.

The present study is primarily motivated by the experiments of Gachelin *et al.*,[40] who devised a microfluidic rheometer based on the deflection of streamlines in the co-flow of a bacterial suspension of *E. coli* and of clear fluid in a rectangular Hele-Shaw geometry. At equal flow rates between the two streams, this deflection is proportional to the viscosity ratio between the two fluids. They also reported a negative particle viscosity in weak flows, followed by an increase to a positive value and eventual shear thinning with increasing flow rate. While these trends agree qualitatively with predictions for bulk suspensions in uniform shear,[20] a direct comparison is difficult owing to the non-uniform distribution achieved by self-propelled particles in confinement: in particular, the tendency of swimmers to spend time in the near-wall high-shear regions in a pressure-driven flow is expected to amplify the effect of activity on the rheology in ways that are not easily anticipated.

In this study, we analyze the effective rheology of a dilute active suspension of self-propelled particles confined between two flat plates and subject to an imposed pressure-driven flow. The theory extends the previous work of Ezhilan and Saintillan,[41] who studied the distribution and transport of self-propelled particles in the same geometry using a continuum model[42,43] but neglected the effect of the hydrodynamic disturbances induced by the swimmers. Here, this effect is taken into account and the modification of the background flow by the particles is used to obtain estimates for the suspension viscosity as a function of flow rate and concentration. Details of the theoretical model are presented in Sec. II, where we also derive an

approximate theory for weak flows and wide channels. Numerical results are discussed in Sec. III where good agreement with experiments is demonstrated.

II. THEORETICAL MODEL

A. Problem definition and Fokker-Planck description

We analyze the effective rheology of a dilute suspension of self-propelled slender particles of length ℓ and aspect ratio r placed between two planar parallel walls in a Newtonian fluid with shear viscosity μ (Fig. 1). The suspension is subject to an imposed pressure-driven Poiseuille flow, whose velocity field in the absence of particles is given by

$$\mathbf{U}(z) = U_m[1 - (z/H)^2]\hat{\mathbf{y}}, \tag{1}$$

where $2H$ denotes the gap width and U_m is the maximum velocity at the centerline ($z = 0$). The corresponding shear rate profile is linear across the channel

$$\Gamma(z) = -\frac{2U_m}{H^2}z. \tag{2}$$

We also introduce the characteristic shear rate $\bar{\Gamma} = U_m/H$, and note that the maximum shear rate at the walls is $2\bar{\Gamma}$. The particles have high aspect ratio ($r \gg 1$), and their length ℓ is assumed to be small compared to the channel dimensions so that it can be effectively neglected: $\ell \ll H$. The distribution of particles inside the channel is described according to classic models[42–44] by the probability density function $\Psi(\mathbf{x}, \mathbf{p}, t)$ of finding a particle at position $\mathbf{x}$ with unit director $\mathbf{p}$ at time t. It satisfies a Fokker-Planck equation

$$\frac{\partial \Psi}{\partial t} + \nabla_x \cdot (\dot{\mathbf{x}}\Psi) + \nabla_p \cdot (\dot{\mathbf{p}}\Psi) = 0, \tag{3}$$

where $\dot{\mathbf{x}}$ and $\dot{\mathbf{p}}$ denote the translational and angular flux velocities and are modeled as

$$\dot{\mathbf{x}} = V_0\mathbf{p} + \mathbf{u} - d_t\nabla_x \ln \Psi, \tag{4}$$

$$\dot{\mathbf{p}} = \zeta(\mathbf{I} - \mathbf{pp}) \cdot \mathbf{E} \cdot \mathbf{p} + \frac{1}{2}\Omega \times \mathbf{p} - d_r\nabla_p \ln \Psi. \tag{5}$$

Here, V_0 is the swimming velocity of an isolated particle, and d_t and d_r denote the translational and rotational Brownian diffusion coefficients, which are assumed to be constant and isotropic. The velocity $\mathbf{u}$ entering the fluxes is the total fluid velocity, which is the sum of the imposed flow $\mathbf{U}(\mathbf{x})$ of Eq. (1) and of the disturbance velocity $\mathbf{u}^d(\mathbf{x}, t)$ due to the presence of the

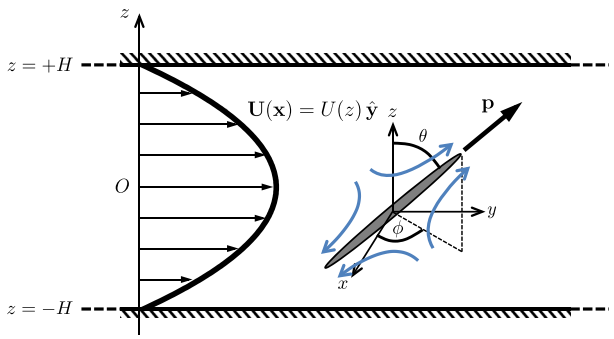

FIG. 1. Problem definition: a dilute suspension of self-propelled particles (with swimming director $\mathbf{p}$) is placed in a plane Poiseuille flow with velocity $\mathbf{U}(\mathbf{x})$ between two parallel flat plates separated by $2H$. The arrows surrounding the particle show the direction of the disturbance flow for a pusher ($\sigma_0 < 0$).

particles, whose calculation is detailed in Sec. II B. The angular flux arises due to the rate-of-strain tensor $\mathbf{E} = (\nabla\mathbf{u} + \nabla\mathbf{u}^t)/2$ and vorticity $\mathbf{\Omega} = \nabla \times \mathbf{u}$; it involves the Bretherton constant ζ,[45] which for a spheroidal particle is given by $\zeta = (r^2 - 1)/(r^2 + 1)$.

We focus here on the case of a dilute suspension, defined as $n\ell^3 \ll 1$ where n is the mean number density. In this limit, the distribution of particles is expected to be homogeneous in the x and y directions, and the disturbance velocity simplifies to $\mathbf{u}^d(\mathbf{x}, t) = u^d(z, t)\hat{\mathbf{y}}$. At steady state, Eqs. (3)–(5) can then be rewritten as

$$V_0 \cos\theta \frac{\partial \Psi}{\partial z} - d_t \frac{\partial^2 \Psi}{\partial z^2} + \zeta\gamma(z)\nabla_p \cdot [(\mathbf{I} - \mathbf{pp}) \cdot \hat{\mathbf{y}} \cos\theta \Psi] = d_r \nabla_p^2 \Psi, \tag{6}$$

where $\gamma(z) = \Gamma(z) + du^d/dz$ is the total shear rate. Eq. (6) expresses the balance of self-propulsion and translational diffusion in the z direction, shear alignment by the local flow, and rotational diffusion. It is subject to a no-flux boundary condition at both channel walls[41]

$$\dot{\mathbf{x}} \cdot \hat{\mathbf{z}} = 0, \quad \text{i.e.,} \quad d_t \frac{\partial \Psi}{\partial z} = V_0 \cos\theta \, \Psi \quad \text{at } z = \pm H. \tag{7}$$

Finally, the probability density function Ψ is normalized as

$$\frac{1}{2H} \int_{-H}^{H} \int_{\Omega} \Psi(z, \mathbf{p}) \, d\mathbf{p} \, dz = n, \tag{8}$$

where Ω denotes the unit sphere of orientation.

B. Particle extra stress and disturbance flow

The calculation of the disturbance flow and of effective rheological properties requires modeling of the particle extra stress, which includes contributions from active dipolar stresses due to self-propulsion, from Brownian motion, and from the imposed flow: $\Sigma^p(z) = \Sigma^a + \Sigma^b + \Sigma^f$. Following Saintillan,[20] each term is modeled as

$$\Sigma^a(z) = n\sigma_0 \left[\langle \mathbf{pp} \rangle - \frac{\langle \mathbf{I} \rangle}{3} \right], \tag{9}$$

$$\Sigma^b(z) = 3nk_BT \left[\langle \mathbf{pp} \rangle - \frac{\langle \mathbf{I} \rangle}{3} \right], \tag{10}$$

$$\Sigma^f(z) = n\ell^3 A\mu\gamma(z) \left[\langle \mathbf{pppp} \rangle - \frac{\mathbf{I}}{3} \langle \mathbf{pp} \rangle \right] : \hat{\mathbf{y}}\hat{\mathbf{z}}, \tag{11}$$

where angle brackets $\langle \cdot \rangle$ denote the orientational average

$$\langle h(\mathbf{p}) \rangle = \frac{1}{n} \int_{\Omega} h(\mathbf{p}) \Psi(z, \mathbf{p}) \, d\mathbf{p}. \tag{12}$$

The active stress Σ^a arises from the force dipoles that neutrally buoyant self-propelled particles exert on the fluid[17] and involves the stresslet strength σ_0, which is negative for pushers[16] such as *E. coli* and *B. subtilis* and positive for pullers[14,15] such as *C. reinhardtii*. The case of $\sigma_0 = 0$ describes hypothetical particles known as movers that swim but do not exert active stresses. The Brownian stress Σ^b arises from Brownian rotations of the particles and involves the thermal energy unit k_BT. Finally, Σ^f is a passive dissipative stress resulting from the inextensibility of the particles in the local strain field $\mathbf{E} = \gamma(z)\hat{\mathbf{y}}\hat{\mathbf{z}}$ that they experience.[29] The dimensionless constant A depends on the shape of the particles; for high-aspect-ratio particles ($r \gg 1$), it is obtained from slender-body theory[27,46] as $A = \pi/6 \log(2r)$.

Knowledge of the stress distribution across the channel allows one to solve for the disturbance fluid velocity, which satisfies the Stokes equations: $-\mu\nabla^2\mathbf{u}^d + \nabla q^d = \nabla\cdot\Sigma^p$, $\nabla\cdot\mathbf{u}^d = 0$, where q^d is the disturbance pressure. Straightforward integration provides an expression for the velocity in terms of the particle shear stress as

$$u^d(z) = -\frac{1}{\mu}\int_{-H}^{z}\Sigma^p_{yz}(z')\,dz', \tag{13}$$

which scales linearly with $n\ell^3$ in the dilute limit. As a result, inclusion of the mean-field disturbance velocity into the Smoluchowski equation for the particle distribution ensures asymptotic accuracy of our model to order $(n\ell^3)^2$. In addition to the flow field, a disturbance pressure gradient is also established in the cross-stream direction as a result of normal stresses: $q^d(z) = \Sigma^p_{zz}(z) + q^d_0$.

Equations (9)–(11) can also be used to estimate the modification of the solvent viscosity by the particles. First, we define a local particle viscosity $\eta_p(z)$ based on a generalized Newtonian model as

$$\eta_p(z) = \frac{\Sigma^p_{yz}(z)}{\gamma(z)} = \frac{n(3k_BT+\sigma_0)\langle p_y p_z\rangle}{\Gamma(z)+du^d/dz} + \mu n\ell^3 A\langle p_y^2 p_z^2\rangle. \tag{14}$$

For convenient comparison with the experiments, it is also useful to introduce a global measure of the particle viscosity that is independent of z. To this end, we follow the approach of Gachelin *et al.*[40] and consider the modification of the net flow rate in the channel by the particles. The imposed flow rate per unit width in the absence of particles is given by

$$\dot{Q}_i = \int_{-H}^{H} U(z)\,dz = \frac{4}{3}U_m H, \tag{15}$$

whereas the disturbance flow rate due the presence of the particles is

$$\dot{Q}_d = \int_{-H}^{H} u^d(z)\,dz. \tag{16}$$

Assuming a Poiseuille law of the form $\dot{Q} = \kappa/\eta$ for the flow rate per unit width, where $\kappa = -(2H^3/3)dq/dy$ and dq/dy is the imposed pressure gradient, we can define a dimensionless relative Newtonian viscosity as the ratio

$$\eta_r = \frac{\dot{Q}_i}{\dot{Q}_i+\dot{Q}_d} = \left[1 + \frac{3}{4U_m H}\int_{-H}^{H} u^d(z)\,dz\right]^{-1}. \tag{17}$$

Clearly, $\eta_r = 1$ in the case of pure solvent ($n\ell^3 = 0$), and departures from this value quantify the effect of the particles on the net viscosity. The effective intrinsic viscosity is then given by

$$[\eta] = \eta_r - 1 = -\frac{\dot{Q}_d}{\dot{Q}_i+\dot{Q}_d}. \tag{18}$$

From this last expression, it becomes obvious that $[\eta] < 0$ corresponds to a positive disturbance flow rate, i.e., a suspension in which particles enhance the imposed flow.

C. Non-dimensionalization

In the following, we scale all variables using time scale d_r^{-1}, length scale H, and velocity scale Hd_r. The probability density function Ψ is also scaled by the number density n. Upon non-dimensionalization, the Fokker-Planck equation (6) becomes

$$Pe_s \cos\theta \frac{\partial \Psi}{\partial z} - 2\Lambda Pe_s^2 \frac{\partial^2 \Psi}{\partial z^2} + \frac{1}{2}\zeta\gamma(z)\nabla_p \cdot [(\mathbf{I} - \mathbf{pp}) \cdot \hat{\mathbf{y}} \cos\theta \Psi] = \frac{1}{2}\nabla_p^2 \Psi, \tag{19}$$

with $\gamma(z) = -Pe_f\, z + du^d/dz$, subject to the boundary conditions

$$\frac{\partial \Psi}{\partial z} = \frac{\cos\theta}{2\Lambda Pe_s}\Psi \quad \text{at } z = \pm 1. \tag{20}$$

We have introduced three-dimensionless groups[41]

$$Pe_s = \frac{V_0}{2d_r H}, \quad Pe_f = \frac{2\bar{\Gamma}}{d_r}, \quad \Lambda = \frac{d_t d_r}{V_0^2}. \tag{21}$$

The swimming Péclet number Pe_s is the ratio of the persistence length of swimmer trajectories over the channel width and is a measure of confinement. The flow Péclet number Pe_f is the ratio of the imposed wall shear rate over the rotational diffusivity of the swimmers; equivalently, it is also the ratio of the correlation time d_r^{-1} of swimmer orientations over the characteristic time $(2\bar{\Gamma})^{-1}$ for alignment by the flow. Finally, Λ is a swimmer-specific parameter characterizing the relative magnitude of Brownian diffusion over deterministic swimming. From the boundary condition (20), it is evident that our model is only valid for $\Lambda > 0$, i.e., in the presence of translational diffusion; the limit of $\Lambda = 0$, which involves a singularity in the distribution of particles at the channel boundaries, is therefore not considered in this work but could be addressed using a different model such as that proposed in our recent work.[47]

Non-dimensionalization of the particle shear stress leads to the simple form

$$\Sigma_{yz}^p(z) = \alpha\langle p_y p_z\rangle + \beta\gamma(z)\langle p_y^2 p_z^2\rangle, \tag{22}$$

where we have introduced the dimensionless groups

$$\alpha = \frac{n}{\mu d_r}(\sigma_0 + 3k_B T) \quad \text{and} \quad \beta = n\ell^3 A. \tag{23}$$

Noting that $k_B T \ll |\sigma_0|$ for typical biological swimmers, $\alpha \approx n\sigma_0/\mu d_r$ describes the relative magnitude of active stresses with respect to dissipative processes. Expressions for the dimensionless disturbance velocity $u^d(z)$, local particle viscosity $\eta_p(z)$, and relative viscosity η_r are then easily obtained as

$$u^d(z) = -\int_{-1}^{z} \Sigma_{yz}^p(z')\, dz', \tag{24}$$

and

$$\eta_p(z) = \frac{\alpha\langle p_y p_z\rangle}{-Pe_f\, z + du^d/dz} + \beta\langle p_y^2 p_z^2\rangle, \quad \eta_r = \left[1 + \frac{3}{2Pe_f}\int_{-1}^{1} u^d(z)\, dz\right]^{-1}. \tag{25}$$

D. Approximate theory for weak flows and wide channels

Before proceeding to solve the governing equations numerically, we derive an approximate theory for the viscosities $\eta_p(z)$ and η_r in the limits of weak flows ($Pe_f \to 0$) and wide channels ($Pe_s \to 0$). If the channel is wide, spatial gradients in orientational moments are weak, and we can approximate the distribution function in the form

$$\Psi(z, \mathbf{p}) \approx c(z)\psi(\mathbf{p}; z), \tag{26}$$

where $c(z) = \langle 1 \rangle$ is the concentration profile and where the orientation distribution function $\psi(\mathbf{p}; z)$ is that for an unbounded suspension in uniform simple shear with shear rate $\gamma(z)$. An approximate expression for the concentration in weak flows was previously found by Ezhilan and Saintillan,[41] as

$$c(z) \approx \frac{B[6\Lambda \cosh B + \cosh Bz]}{6\Lambda B \cosh B + \sinh B} \quad \text{with} \quad B^{-1} = \Lambda Pe_s \sqrt{\frac{12}{1+6\Lambda}}. \tag{27}$$

In the limit of weak flow, the orientation distribution $\psi(\mathbf{p}; z)$ can be also calculated asymptotically as a regular expansion in powers of shear rate,[28] leading to the approximation

$$\psi(\mathbf{p}; z) \approx \frac{1}{4\pi} + \frac{\zeta}{8\pi}\gamma(z) p_y p_z + \cdots. \tag{28}$$

The orientational moments are then readily obtained as

$$\langle p_y p_z \rangle \approx \frac{\zeta}{30}\gamma(z)c(z), \quad \langle p_y^2 p_z^2 \rangle \approx \frac{1}{15}c(z). \tag{29}$$

Using Eqs. (27) and (29), it is then straightforward to estimate the dimensionless particle shear stress and local viscosity as

$$\Sigma_{yz}^{p}(z) \approx \frac{1}{30}(\alpha\zeta + 2\beta)c(z)\gamma(z), \quad \eta_p(z) \approx \frac{1}{30}(\alpha\zeta + 2\beta)c(z). \tag{30}$$

In very wide channels and away from walls we have $c(z) \approx 1$, and η_p simplifies to the low-shear-rate asymptote previously derived by Saintillan[20] for a bulk suspension in uniform shear. If we further assume that $\gamma(z) \approx -Pe_f z$, which is valid in very dilute systems, we can also derive an analytical expression for the relative viscosity as

$$\eta_r \approx \left[1 - \frac{1}{10}(\alpha\zeta + 2\beta)\frac{2\sinh B - 2B\cosh B + B^2 \sinh B + 2B^3\Lambda \cosh B}{B^2(6\Lambda B \cosh B + \sinh B)}\right]^{-1}. \tag{31}$$

In very wide channels ($B \to \infty$) and dilute systems ($n\ell^3 \to 0$)

$$\eta_r \to \left[1 - \frac{1}{30}(\alpha\zeta + 2\beta)\right]^{-1} \approx 1 + \frac{1}{30}(\alpha\zeta + 2\beta), \tag{32}$$

which again matches the low-shear-rate asymptote in a bulk suspension.[20] As shown below in Sec. III C, Eq. (31) indeed captures the relative viscosity quantitatively at low concentrations and in wide channels.

E. Numerical solution and parameter selection

Equation (19) subject to boundary conditions (20) was solved numerically for a range of parameter values using a finite-volume numerical algorithm previously developed by Ezhilan and Saintillan.[41] The algorithm solves for the full distribution function in the three-dimensional space $\Omega \times [-1, 1]$ and satisfies the normalization condition of Eq. (8) to machine precision. Due to the nonlinearity of the governing equations, the unsteady version of Eq. (19) was marched explicitly in time to steady state, coupled to a semi-analytical solution for the fluid velocity based on Eq. (24).

Simulation parameters were estimated based on the experiments of Gachelin *et al.*,[40] Rusconi *et al.*,[13] and López *et al.*[31] These studies used *E. coli* bacteria, with body length $\ell \approx 2\,\mu$m, swimming speed $V_0 \approx 20\,\mu\text{m s}^{-1}$, and dipole strength $\sigma_0 \approx -9.46 \times 10^{-19}\,\text{N m}$. The

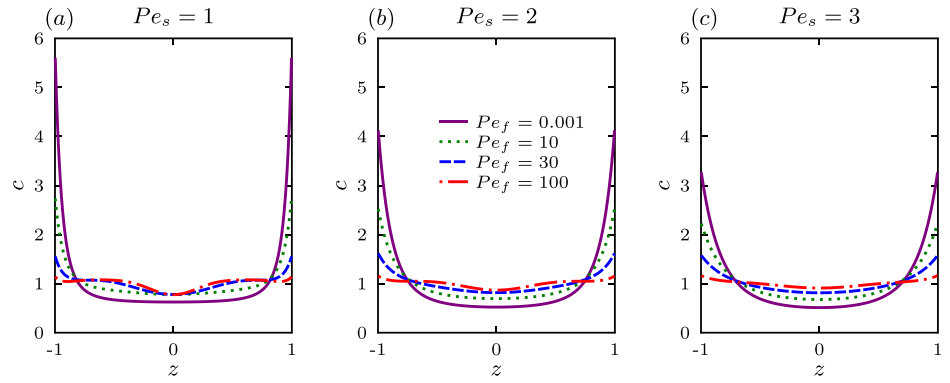

FIG. 2. Concentration profiles for $\Lambda = 0.02$, $\alpha = -5$, $\beta = 1$, different values of Pe_f, and increasing levels of confinement: (a) $Pe_s = 1$, (b) $Pe_s = 2$, and (c) $Pe_s = 3$.

translational and rotational diffusivities were estimated as $d_t \approx 1.6 \times 10^{-11}\,\mathrm{m^2\,s^{-1}}$ and $d_r \approx 0.5\ \mathrm{s^{-1}}$ (based on the tumbling rate of the bacteria). The number density is varied in the range of $n \approx 10^{14}$–$10^{16}\,\mathrm{m^{-3}}$, which is consistent with typical experiments, and the mean shear rate is varied between 0 and $250\,\mathrm{s^{-1}}$. Based on these estimates, the activity parameter α ranges from 1 to 10 in absolute value; we focus in this study on the case of pushers for which $\alpha < 0$, though a few results are also shown for pullers ($\alpha > 0$) as well as movers ($\alpha = 0$). Finally, we set $\zeta = 1$ in all of our calculations, as is appropriate for slender swimmers, and most of the results presented here are for channel half widths of $H = 10\,\mu\mathrm{m}$ and smaller, which is on the lower end of typical experimental values.

III. RESULTS AND DISCUSSION

A. Particle distributions

We first analyze steady-state particle distributions across the channel, with special focus on the orientational moments governing the effective rheology. Some of these results echo those presented in our previous work,[41] but also extend them to higher-order moments and differ slightly due to the inclusion of the disturbance velocity u_d, which was neglected in that prior study. Concentration profiles $c(z) = \langle 1 \rangle$ are illustrated in Fig. 2 and show strong accumulation of particles at the channel walls in agreement with experiments,[8–10,40] numerical simulations,[48–51] and theoretical models.[41,47,52,53] As explained in previous studies, this accumulation is to leading order simply the result of self-propulsion and confinement[41] and is also amplified by hydrodynamic interactions in the case of pusher particles.[8] The influence of the flow and swimming Péclet numbers is also as expected. In particular, increasing Pe_s is equivalent to

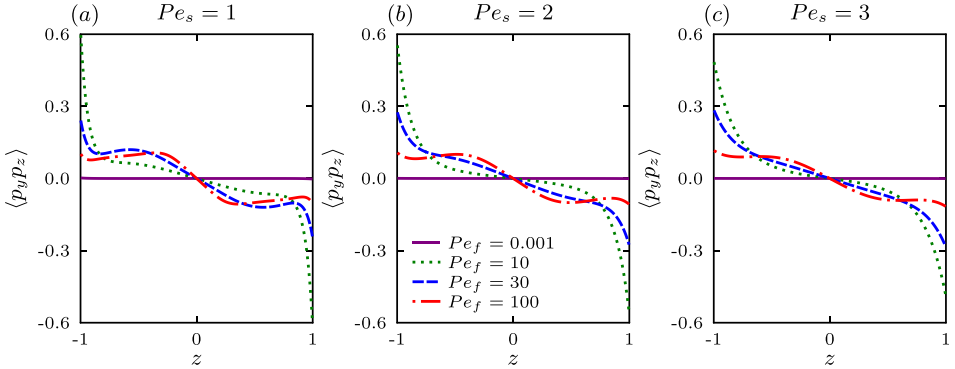

FIG. 3. Profiles of the off-diagonal component $\langle p_y p_z \rangle$ of the nematic order parameter tensor for $\Lambda = 0.02$, $\alpha = -5$, $\beta = 1$, different values of Pe_f, and increasing levels of confinement: (a) $Pe_s = 1$, (b) $Pe_s = 2$, and (c) $Pe_s = 3$.

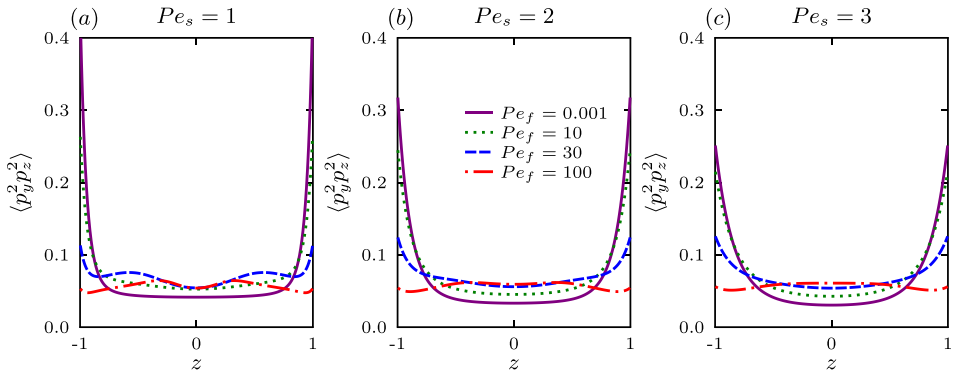

FIG. 4. Profiles of the component $\langle p_y^2 p_z^2 \rangle$ of the fourth-order orientational moment for $\Lambda = 0.02$, $\alpha = -5$, $\beta = 1$, different values of Pe_f, and increasing levels of confinement: (a) $Pe_s = 1$, (b) $Pe_s = 2$, and (c) $Pe_s = 3$.

decreasing the channel width, which results in the interaction and eventual merging of the two accumulation layers. Increasing Pe_f also causes a decrease in accumulation due to the reorientation of the particles by the shear, which limits their ability to swim towards boundaries by reducing the wall-normal polarization.[41] This effect of flow strength was also recently observed in the microfluidic experiments of Figueroa-Morales *et al.*[54] Another effect of increasing Pe_f is the appearance of a weak depletion near the channel centerline, which is also observed in experiments[13] and results from the preferential trapping of the particles in high-shear near-wall regions due to their nematic alignment with the flow. This depletion is most notable in wide channels ($Pe_s = 1$) as rationalized by previous theoretical models.[41,55] The reader is referred to our previous modeling work[41] for a more thorough analysis of these various effects, including the derivation of scaling laws for the thickness of the wall accumulation layer and centerline depletion, as well as their relation to the polarization and nematic parameter fields.

In anticipation of the rheology results discussed in Sec. III C, we turn our attention to the second and fourth orientational moments, which are known to affect the particle shear stress and effective viscosity via Eqs. (22) and (25). The off-diagonal component $\langle p_y p_z \rangle$ of the nematic order parameter tensor, which enters the active contribution to the particle stress, is plotted in Fig. 3 for the same parameters as in Fig. 2. Unsurprisingly, we find that the particles align under the local shear, leading to a net shear nematic alignment across the channel. Upon increasing flow rate, $\langle p_y p_z \rangle$ first increases strongly near the walls, since the concentration and shear rate are both highest there. As Pe_f keeps increasing, the weakening of wall accumulation becomes evident, causing the maximum in shear alignment to shift away from the walls towards the shear-trapping region where the particle concentration is the highest. Corresponding data for the fourth moment $\langle p_y^2 p_z^2 \rangle$, which enters the dissipative contribution to the particle stress, are shown in Fig. 4. This fourth moment, which is always positive, follows trends very

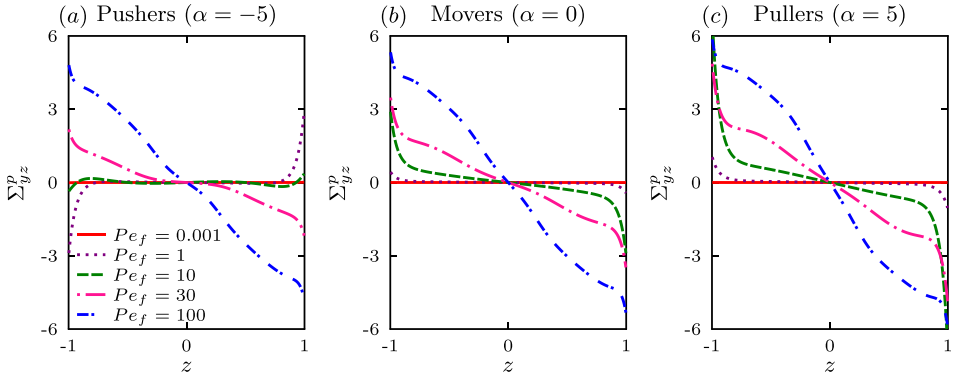

FIG. 5. Particle shear stress profiles $\Sigma_{yz}^p(z)$ for $Pe_s = 1$, $\Lambda = 0.02$, $\beta = 1$ and for different flow strengths Pe_f in the case of: (a) pushers ($\alpha < 0$), (b) movers ($\alpha = 0$), and (c) pullers ($\alpha > 0$).

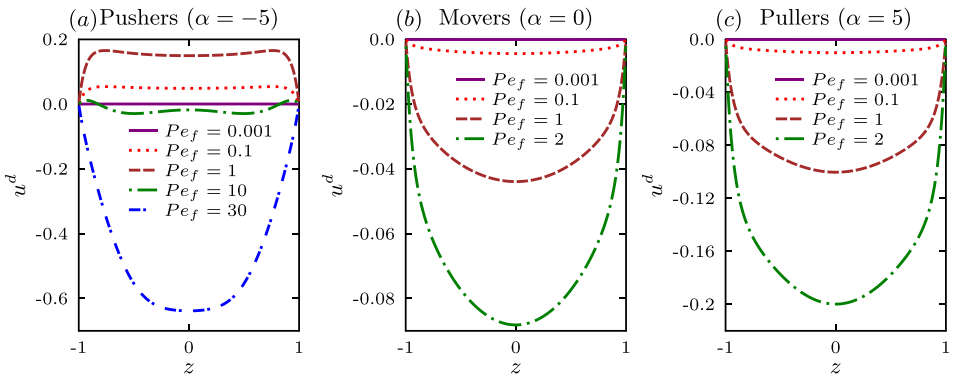

FIG. 6. Disturbance velocity profiles $u^d(z)$ for $Pe_s = 1$, $\Lambda = 0.02$, $\beta = 1$ and for different flow strengths Pe_f in the case of: (a) pushers ($\alpha < 0$), (b) movers ($\alpha = 0$), and (c) pullers ($\alpha > 0$).

similar to the concentration profiles of Fig. 2, in agreement with the weak flow estimate of Eq. (29). In particular, it is sharply peaked near the walls in weak flows but becomes nearly uniform in stronger flows.

B. Particle shear stress and disturbance flow

Both moments $\langle p_y p_z \rangle$ and $\langle p_y^2 p_z^2 \rangle$ calculated above enter the particle shear stress Σ^p_{yz} in Eq. (22), which is plotted in Fig. 5 for pushers, movers, and pullers at different flow strengths. In all cases, the particle shear stress is an odd function of z as expected from symmetry considerations, and its magnitude tends to increase with flow strength as a result of the passive stress $\boldsymbol{\Sigma}^f$, which scales linearly with the local shear rate. The trends in the case of pushers, however, are more complex: we find that the sign of the shear stress changes at a critical flow strength, indicating a change in rheological behavior. This reversal results from the competition between active and dissipative stresses, which are of opposite signs for pushers, and will be discussed in more detail below. Movers and pullers, however, do not exhibit this reversal and behave in a qualitatively similar way.

These trends on the particle stress are easier to interpret in terms of the disturbance flow profiles, which are obtained by integration of Σ^p_{yz} according to Eq. (24) and plotted in Fig. 6. In the case of movers and pullers in Figs. 6(b) and 6(c), the disturbance velocity is always negative across the entire channel and has a roughly parabolic profile, indicating that the effect of the particles is to slow down the imposed pressure-driven flow, as would be expected in the case of passive rodlike particles.[28,56] This effect, which becomes stronger with increasing Pe_f, can be interpreted as an increase in the effective shear viscosity due to the particles, which results from both passive stresses and active stresses in the case of pullers. This explains, in particular, why the disturbance flow is stronger for pullers than movers. The case of pushers in Fig. 6(a), however, is more complex and interesting. In weak flows, the disturbance velocity is positive suggesting an enhancement of the flow rate with respect to the imposed flow; this will be confirmed in Sec. III C where we report relative viscosities below one. This enhancement is the result of active stresses, which are strongest in the near-wall accumulation layer in weak flows as shown in Fig. 3; consequently, the profiles are nearly flat in the bulk of the channels with sharp gradients near the walls. Above a certain flow strength, the disturbance velocity decreases to become negative as active stresses become weaker and the effect of dissipative stresses is more significant; this non-monotonic trend will be reflected in the viscosity data below. The profile shape also becomes more parabolic in strong flows owing to the nearly linear particle shear stress distribution in this case.

C. Effective rheology

We now turn to the effective rheology of the suspension, first considering the local particle viscosity $\eta_p(z)$, which is plotted in Fig. 7. Unsurprisingly, the local viscosity varies across the channel due to the combined effects of confinement and non-uniform shear rate, both of which

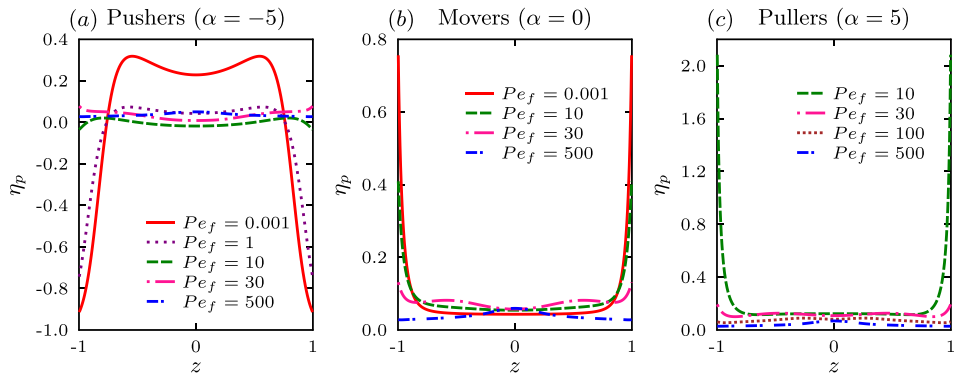

FIG. 7. Local particle viscosity profiles $\eta_p(z)$ for $Pe_s = 1, \Lambda = 0.02, \beta = 1$ and different values of Pe_f for: (a) pushers, (b) movers, and (c) pullers.

affect the local orientation distribution. In suspensions of movers and pullers in Figs. 7(b) and 7(c), the particle viscosity is found to be positive everywhere in the channel. In weak flows, it is maximum near the walls due to the strong particle accumulation and strong shear rate there. As the flow strength increases, shear-thinning is observed as in the classic case of passive rod-like particles[28] though it occurs predominantly near the walls, eventually leading to a weak maximum in the viscosity near the centerline at high values of Pe_f; this is consistent with the standard explanation of shear-thinning in rod suspensions due to the nematic alignment of the particles with the flow, which is strongest in the high-shear near-wall regions but negligible at the centerline where the shear rate vanishes. The case of pushers is illustrated in Fig. 7(a). In weak flows, the particle viscosity is strongly negative close to the boundaries but slightly positive in the low-shear regions close to the centerline; this explains the enhancement of the flow and the plug-like disturbance velocity profiles observed in Fig. 6(a). At intermediate Pe_f, the viscosity becomes positive near the channel walls due to the strong nematic alignment of the particles there, which causes the passive contribution to the stress to dominate the active contribution in Eq. (22), though it remains negative near the centerline where the shear rate is weak. This change in sign explains the non-monotonicity of the velocity profiles in Fig. 6(a): for a given pressure gradient, the flow is hindered near the walls where $\eta_p > 0$, whereas it is enhanced near the centerline where $\eta_p < 0$ (see the curve for $Pe_f = 10$). In strong flows, the local viscosity becomes positive throughout the channel due to passive stresses and reaches its maximum at the centerline.

The net effect of these results on the flow rate is summarized in Fig. 8, showing the relative viscosity η_r as a function of the various parameters. Fig. 8(a) illustrates the effect of flow strength and activity: in suspensions of movers and pullers, shear-thinning is observed with increasing flow rate as occurs in passive rod suspensions; the relative viscosity, however, is enhanced by activity in the case of pullers as known from previous models[20] and experiments.[38,39] The case of pushers shows a non-monotonic dependence on flow rate: in weak flows, active stresses dominate resulting in a relative viscosity below one; as flow rate increases, the dissipative stresses become stronger leading to an increase in η_r, which becomes greater than one and eventually shear-thins in very strong flows. These trends are all consistent with the experiments of Gachelin *et al.*[40] and López *et al.*,[31] and also agree qualitatively with previous bulk models.[20] Confinement, however, has a quantitative effect as depicted in Fig. 8(b) showing the same results in the case of pushers but for different values of Pe_s. The effect is found to be stronger in weak flows, where increasing confinement reduces the effect of activity: this is primarily the consequence of the merging of the accumulation layers and flattening of the concentration profile, which drives more particles towards the center of the channel where the shear rate is weaker.

The effect of number density n is described in Figs. 8(c) and 8(d), with the caveat that our model is based on a dilute assumption and therefore may not be accurate at high concentrations.

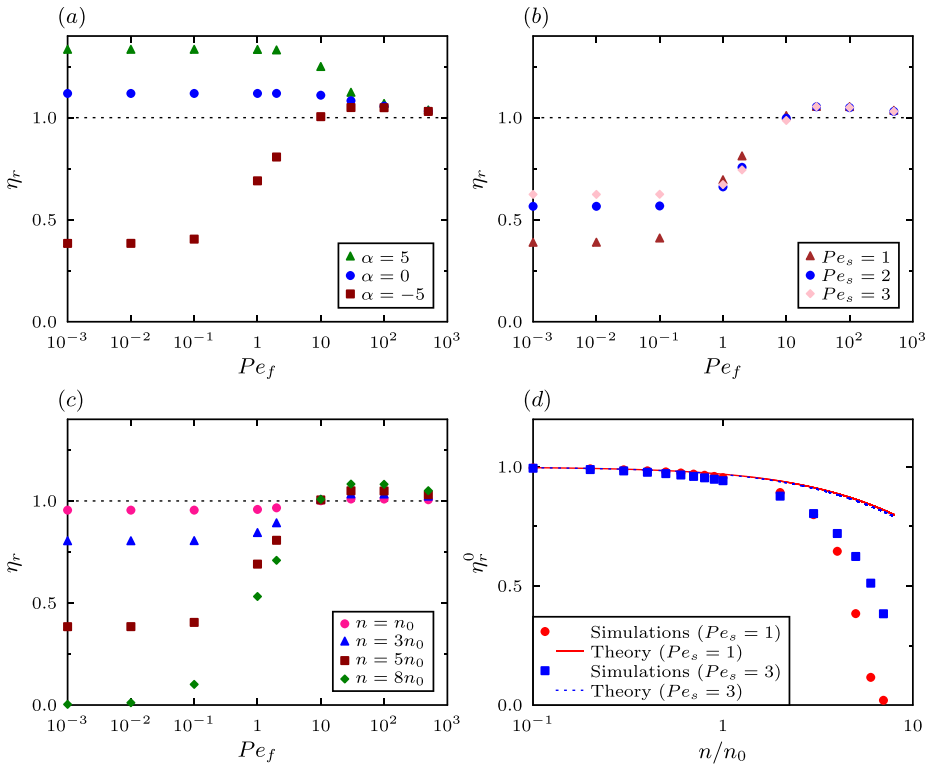

FIG. 8. (a) Relative viscosity η_r for $Pe_s = 1$, $\Lambda = 0.02$ and $\beta = 1$ as a function of flow rate Pe_f for pullers, movers, and pushers. (b) Effect of confinement on η_r in the case of pushers ($\alpha = -5$). (c) Effect of number density n on η_r in the case of pushers. In this plot, the ratio $\alpha/\beta = -5$ is kept fixed while varying n; the reference number density n_0 corresponds to $\alpha = -1$. (d) Effect of number density n on the low-Pe_f Newtonian asymptote η_r^0, and comparison to the theoretical estimate of Eq. (31).

In Fig. 8(c), the number density n is varied while keeping the ratio of the two parameters α and β constant. As expected, increasing density enhances the effect of both active stresses (at low flow rates) and passive stresses (at high flow rates), leading to more pronounced departures from case of pure solvent ($\eta_r = 1$). The transition from $\eta_r < 1$ to $\eta_r > 1$, however, always occurs at a fixed flow rate of $Pe_f \approx 10$ for this choice of parameters, regarding of density. In the low-Pe_f regime, we find that the Newtonian plateau for η_r decreases monotonically with n in the case of pushers, eventually reaching zero at high concentrations. Both of these observations are consistent with the recent experiments of López *et al.*[31] in a cylindrical Couette flow, who measured very similar trends as in Fig. 8(c) and also reported an apparent transition to superfluidity at high densities. This transition to negative total viscosities is expected to lead to instabilities and is related to the previously reported emergence of unidirectional flows in confined active suspensions.[32–36] In the experiments of López *et al.*,[31] the transition to superfluidity occurred at a number density $n \approx 8 \times 10^{15}\,\mathrm{m}^{-3}$, from which we can estimate the value of the ratio n/n_0 for the transition as

$$\left(\frac{n}{n_0}\right)_{\eta_r=0} \approx \frac{|\sigma_0| n}{\mu d_r} = \frac{7.98 \times 10^{-19} \times 8 \times 10^{15}}{1.4 \times 10^{-3} \times 0.5} \approx 9.1, \tag{33}$$

where we have used the estimate of $\sigma_0 = -7.98 \times 10^{-19}\,\mathrm{N\,m}$ for the dipole strength as measured by Drescher *et al.*[16] in the case of *E. coli*. The result of Eq. (33) is reasonably close to the value of 8 predicted by our model in Fig. 8(c), suggesting that the validity of the model might in fact extend beyond the strict dilute limit. Fig. 8(d) shows more details on the dependence of the low-Pe_f viscosity plateau on number density and also compares the numerical results to the

theoretical estimate of Eq. (31). This estimate captures the initial decrease in viscosity quite well, especially in wider channels ($Pe_s = 1$) as anticipated; however, significant quantitative departures are observed at higher number densities.

IV. CONCLUSIONS

We have developed a nonlinear mean-field kinetic theory for the configuration and effective rheology of a dilute active suspension in planar Poiseuille flow that accounts for the hydrodynamic disturbance driven by the particles as a result of both active and passive stresses. This model links together our previous theories for the rheology of bulk active suspensions in uniform shear[20] and for the distribution of particles in Poiseuille flow in the absence of hydrodynamic disturbances.[41] The rheological trends we predicted agree qualitatively with prior bulk models as well as experiments on bacterial suspensions, both in the bulk[31] and in microfluidic geometries.[40] In particular, we have confirmed that the effects of activity are predominant in weak flows, where pushers tend to decrease the viscosity whereas pullers increase it; in strong flows, activity becomes negligible and the suspension behavior is similar to that of passive rodlike particles. Confinement, however, has a nontrivial quantitative influence on the viscosity as a result of two main effects: the non-homogeneous distribution of particles across the channel with strong accumulation near the walls in weak flows, and the non-uniform shear profile of the imposed pressure-driven flow controlling particle alignment. Notably, this tends to enhance the impact of the particles on the flow in weak flows compared to a bulk system. Finally, our dilute model was able to capture the decrease in viscosity in pusher suspensions with increasing volume fraction, which led to the transition to superfluidity in the experiments of López *et al.*:[31] while good agreement between experiments and model predictions was found, a more quantitative description of this transition, however, is beyond the range of applicability of the present theory and may require more realistic particle simulations such as those of Saintillan and Shelley,[57,58] whose validity extends into the semi-dilute regime.

ACKNOWLEDGMENTS

We thank Anke Lindner and Eric Clément for useful conversations, and gratefully acknowledge the support from NSF Grants Nos. CBET-1532652 and DMS-1463965.

[1]S. S. Suarez and A. A. Pacey, Hum. Reprod. Update **12**, 23 (2006).
[2]P. Denissenko, V. Kanstler, D. J. Smith, and J. Kirkman-Brown, Proc. Natl. Acad. Sci. U.S.A. **109**, 8007 (2012).
[3]V. Kantsler, J. Dunkel, M. Blayney, and R. E. Goldstein, eLife **3**, 02403 (2014).
[4]P. Galajda, J. Keymer, P. Chaikin, and R. Austin, J. Bacteriol. **189**, 8704 (2007).
[5]S. E. Hulme, W. R. DiLuzio, S. S. Shevkoplyas, L. Turner, M. Mayer, H. C. Berg, and G. M. Whitesides, Lab Chip **8**, 1888 (2008).
[6]G. Lambert, D. Liao, and R. H. Austin, Phys. Rev. Lett. **104**, 168102 (2010).
[7]E. Altshuler, G. Miño, C. Pérez-Penichet, L. del Río, A. Lindner, A. Rousselet, and E. Clément, Soft Matter **9**, 1864 (2013).
[8]A. P. Berke, L. Turner, H. C. Berg, and E. Lauga, Phys. Rev. Lett. **101**, 038102 (2008).
[9]G. Li and J. X. Tang, Phys. Rev. Lett. **103**, 078101 (2009).
[10]G. Li, J. Bensson, L. Nisimova, D. Munger, P. Mahautmr, J. X. Tang, M. R. Maxey, and Y. V. Brun, Phys. Rev. E **84**, 041932 (2011).
[11]J. Hill, O. Kalkanci, J. L. McMurry, and H. Koser, Phys. Rev. Lett. **98**, 068101 (2007).
[12]T. Kaya and H. Koser, Biophys. J. **102**, 1514 (2012).
[13]R. Rusconi, J. S. Guasto, and R. Stocker, Nat. Phys. **10**, 212 (2014).
[14]K. Drescher, R. E. Goldstein, N. Michel, M. Polin, and I. Tuval, Phys. Rev. Lett. **105**, 168101 (2010).
[15]J. S. Guasto, K. A. Johnson, and J. P. Gollub, Phys. Rev. Lett. **105**, 168102 (2010).
[16]K. Drescher, J. Dunkel, L. H. Cisneros, S. Ganguly, and R. E. Goldstein, Proc. Natl. Acad. Sci. U.S.A. **108**, 10940 (2011).
[17]Y. Hatwalne, S. Ramaswamy, M. Rao, and R. Aditi Simha, Phys. Rev. Lett. **92**, 118101 (2004).
[18]B. M. Haines, I. S. Aranson, L. Berlyand, and D. A. Karpeev, Phys. Biol. **5**, 046003 (2008).
[19]B. M. Haines, A. Sokolov, I. S. Aranson, L. Beryland, and D. A. Karpeev, Phys. Rev. E **80**, 041922 (2009).
[20]D. Saintillan, Exp. Mech. **50**, 1275 (2010).
[21]D. Saintillan, Phys. Rev. E **81**, 056307 (2010).
[22]S. Heidenreich, S. Hess, and S. H. L. Klapp, Phys. Rev. E **83**, 011907 (2011).
[23]S. D. Ryan, B. M. Haines, L. Berlyand, F. Siebert, and I. S. Aranson, Phys. Rev. E **83**, 050904 (2011).
[24]Y. Bozorg and P. T. Underhill, Rheol. Acta **53**, 899 (2014).
[25]M. G. Forest, P. Phuworawong, Q. Wang, and R. Zhou, Philos. Trans. R. Soc. A **372**, 20130362 (2014).

[26]M. Moradi and A. Najafi, Europhys. Lett. **109**, 24001 (2015).
[27]G. K. Batchelor, J. Fluid Mech. **46**, 813 (1971).
[28]H. Brenner, Int. J. Multiphase Flow **1**, 195 (1974).
[29]E. J. Hinch and L. G. Leal, J. Fluid Mech. **76**, 187 (1976).
[30]A. Sokolov and I. S. Aranson, Phys. Rev. Lett. **103**, 148101 (2009).
[31]H. M. López, J. Gachelin, C. Douarche, H. Auradou, and E. Clément, Phys. Rev. Lett. **115**, 028301 (2015).
[32]A. Creppy, F. Plouraboué, O. Praud, X. Druart, S. Cazin, H. Yu, and P. Degond, "Symmetry-breaking phase-transitions in highly concentrated semen" (unpublished).
[33]H. Wioland, E. Lushi, and R. E. Goldstein, "Directed collective motion of bacteria under channel confinement," N. J. Phys. (submitted).
[34]R. Voituriez, J. F. Joanny, and J. Prost, Europhys. Lett. **70**, 404 (2005).
[35]M. Ravnik and J. M. Yeomans, Phys. Rev. Lett. **110**, 026001 (2013).
[36]M. Theillard, B. Ezhilan, R. Alonso-Matilla, and D. Saintillan, "Geometric control of active collective motion," Soft Matter (submitted).
[37]G. Subramanian and D. L. Koch, J. Fluid Mech. **632**, 359 (2009).
[38]S. Rafaï, L. Jibuti, and P. Peyla, Phys. Rev. Lett. **104**, 098102 (2010).
[39]A. G. McDonnell, T. C. Gopesh, J. Lo, M. O'Bryan, L. Y. Yeo, J. R. Friend, and R. Prabhakar, Soft Matter **11**, 4658 (2015).
[40]J. Gachelin, G. Miño, H. Berthet, A. Lindner, A. Rousselet, and E. Clément, Phys. Rev. Lett. **110**, 268103 (2013).
[41]B. Ezhilan and D. Saintillan, J. Fluid Mech. **777**, 482 (2015).
[42]D. Saintillan and M. J. Shelley, Phys. Fluids **20**, 123304 (2008).
[43]D. Saintillan and M. J. Shelley, C. R. Phys. **14**, 497 (2013).
[44]D. Saintillan and M. J. Shelley, Phys. Rev. Lett. **100**, 178103 (2008).
[45]F. P. Bretherton, J. Fluid Mech. **14**, 284 (1962).
[46]G. K. Batchelor, J. Fluid Mech. **44**, 419 (1970).
[47]B. Ezhilan, R. Alonso-Matilla, and D. Saintillan, J. Fluid Mech. **781**, R4 (2015).
[48]J. P. Hernández-Ortiz, C. G. Stoltz, and M. D. Graham, Phys. Rev. Lett. **95**, 204501 (2005).
[49]R. W. Nash, R. Adhikari, J. Tailleur, and M. E. Cates, Phys. Rev. Lett. **104**, 258101 (2010).
[50]A. Costanzo, R. Di Leonardo, G. Ruocco, and L. Angelani, J. Phys.: Condens. Matter **24**, 065101 (2012).
[51]S. Chilukuri, C. H. Collins, and P. T. Underhill, J. Phys.: Condens. Matter **26**, 115101 (2014).
[52]C. F. Lee, New J. Phys. **15**, 055007 (2013).
[53]J. Elgeti and G. Gompper, Europhys. Lett. **109**, 58003 (2015).
[54]N. Figueroa-Morales, G. Miño, A. Rivera, R. Caballero, E. Clément, E. Altshuler, and A. Lindner, Soft Matter **11**, 6284 (2015).
[55]R. N. Bearon and A. L. Hazel, J. Fluid Mech. **771**, R3 (2015).
[56]R. L. Schiek and E. S. G. Shaqfeh, J. Fluid Mech. **296**, 271 (1995).
[57]D. Saintillan and M. J. Shelley, Phys. Rev. Lett. **99**, 058102 (2007).
[58]D. Saintillan and M. J. Shelley, J. R. Soc. Interface **9**, 571 (2012).